JPET Fast Forward. Published on September 7, 2017 as DOI: 10.1124/jpet.117.242909
This article has not been copyedited and formatted. The final version may differ from this version.

JPET #242909

Acalabrutinib (ACP-196): A covalent Bruton tyrosine kinase (BTK) inhibitor with a differentiated selectivity and in vivo potency profile

Tjeerd Barf, Todd Covey, Raquel Izumi, Bas van de Kar, Michael Gulrajani, Bart van Lith, Maaike van Hoek, Edwin de Zwart, Diana Mittag, Dennis Demont, Saskia Verkaik, Fanny Krantz, Paul G. Pearson, Roger Ulrich and Allard Kaptein

Acerta Pharma BV, Oss, The Netherlands

JPET Fast Forward. Published on September 7, 2017 as DOI: 10.1124/jpet.117.242909
This article has not been copyedited and formatted. The final version may differ from this version.

JPET #242909

Running Title: Acalabrutinib, a differentiated covalent BTK inhibitor

Corresponding Author: Tjeerd Barf, Acerta Pharma BV, Kloosterstraat 9, 5349 AB Oss, The Netherlands. E-mail: t.barf@acerta-pharma.com. Tel. +31 412 700 574

Number of text pages: 59

Number of Tables: 3

Number of Figures: 5

Number of References: 43

Word count Abstract: 232

Word count Introduction: 513

Word count Discussion: 1548

Abbreviations: ADCC, antibody-dependent cellular cytoxicity; AUC, area under the concentration-time curve; BCR, B-cell receptor; BLK, B-lymphocyte kinase; BMX, bone marrow tyrosine kinase gene in chromosome X; BTK, Bruton's tyrosine kinase; CLL, chronic lymphocytic leukemia; ErbB, erythroblastosis oncogene B; EGFR (ErbB1), epidermal growth factor receptor; FACS, fluorescence-activated cell sorter; FBS, fetal bovine serum; FGR, Gardner-Rasheed feline sarcoma viral (v-fgr) oncogene homolog; FYN, Fgr/Yes related novel protein; HCK, hemopoietic cell kinase; hWB, human whole blood; IL, interleukin; IMAP, immobilized metal affinity for phosphochemicals; ITK, IL2-inducible T-cell kinase; JAK, janus-associated kinase; LCK, lymphocyte-specific protein tyrosine kinase; LYN, Lck/Yes novel; PBMC, peripheral blood mononuclear cell; PBS, phosphate-buffered saline; PD, pharmacodynamics; PK, pharmacokinetics; SRC, Rous sarcoma oncogene cellular homologue; SRR, structure-reactivity relationship; TEC, tyrosine kinase expressed in hepatocellular carcinoma; Txk, T and X cell expressed kinase; XLA, X-linked agammaglobulinemia; YES, Yamaguchi sarcoma viral oncogene homologue.

Abstract

Several small-molecule BTK inhibitors are in development for B-cell malignancies and autoimmune disorders, each characterized by distinct potency and selectivity patterns. Herein we describe the pharmacologic characterization of BTK inhibitor acalabrutinib (**1**, ACP-196). Acalabrutinib possesses a reactive butynamide group that binds covalently to Cys481 in BTK. Relative to the other BTK inhibitors described here, the reduced intrinsic reactivity of acalabrutinib helps to limit inhibition of off-target kinases having cysteine-mediated covalent binding potential. Acalabrutinib demonstrated higher biochemical and cellular selectivity than ibrutinib (**2**) and spebrutinib (**3**). Importantly, off-target kinases that have been associated with adverse effects, such as EGFR and ITK, are not inhibited. Determination of the inhibitory potential of anti-IgM-induced CD69 expression in human PBMC and whole blood demonstrate that acalabrutinib is a potent functional BTK inhibitor. In vivo evaluation in mice revealed that acalabrutinib is more potent than ibrutinib and spebrutinib. Preclinical and clinical studies showed that the level and duration of BTK occupancy correlate with in vivo efficacy. Evaluation of the pharmacokinetic properties of acalabrutinib in healthy adult volunteers demonstrated rapid absorption and fast elimination. In these healthy individuals, a single oral dose of 100 mg showed approximately 99% median target coverage at 3 and 12 hours, and around 90% at 24 hours in peripheral B cells. In conclusion, acalabrutinib is a BTK inhibitor with key pharmacologic differentiators versus ibrutinib and spebrutinib, and is currently being evaluated in clinical trials.

JPET Fast Forward. Published on September 7, 2017 as DOI: 10.1124/jpet.117.242909
This article has not been copyedited and formatted. The final version may differ from this version.

INTRODUCTION

Bruton tyrosine kinase (BTK) is a TEC family non-receptor protein kinase expressed in B cells, myeloid cells, mast cells and platelets. B-cell receptor (BCR)-mediated signaling is essential for activation, proliferation and survival of B lymphocytes, and BTK is an essential component of the BCR signaling cascade (Hendriks et al., 2014). Expression of BTK in B-cell leukemias and lymphomas has also been reported (de Weers et al., 1993; Katz et al., 1994). Furthermore, BTK is involved in the regulation of FcγR signaling in myeloid cells (Jongstra-Bilen et al., 2008), and in mast cell degranulation following FcεR1 activation (Ellmeijer et al., 2011). These features of BTK render it a very attractive target in treating B-cell malignancies (Hendriks et al., 2014) and autoimmune disease (Whang and Chang, 2014). Several small-molecule inhibitors of BTK have progressed to the clinic (Table 1), and collectively demonstrate clinical validation of BTK inhibition in B-cell malignancies. Most of the BTK inhibitors listed in Table 1 have been reported to bind in a covalent fashion to a cysteine residue (Cys481) at the rim of the ATP-binding pocket of BTK (Norman 2016; Pan et al., 2007). To date, ibrutinib is the only BTK inhibitor that has received marketing authorization for the treatment of B-cell malignancies (Ponader and Burger, 2014); however, it is associated with adverse events not likely due to inhibition of BTK function based on clinical observations in X-linked agammaglobulinemia (XLA) patients having dysfunctional BTK (Winkelstein et al., 2006). These ibrutinib-mediated adverse events include rash, diarrhea, arthralgias or myalgias, atrial fibrillation and major hemorrhage (Wang et al., 2013; Byrd et al., 2013; O'Brien et al., 2014), some of which may be explained by inhibition of off-target kinases EGFR, TEC, ITK and TXK (Honigberg et al., 2010). Spebrutinib is another covalent BTK inhibitor that was subject to clinical evaluation, and although reportedly a highly selective inhibitor (Evans et al., 2013), doses needed to achieve a partial response in patients with relapsed/refractory CLL/SLL are higher than for ibrutinib (Brown et al., 2016).

Here we report the differentiated profile of BTK inhibitor acalabrutinib (ACP-196, **1**, 4-[8-amino-3-[(2S)-1-but-2-ynoylpyrrolidin-2-yl]imidazo[1,5-a]pyrazin-1-yl]-N-(2-pyridyl)benzamide). Acalabrutinib is a small-molecule irreversible BTK inhibitor (Figure 1) that shows encouraging clinical activity and safety in relapsed/refractory CLL patients (Byrd et al., 2016). The preclinical profile of acalabrutinib and a few additional compounds was compared with ibrutinib (PCI-32765, **2**) and spebrutinib (CC-292, **3**) to

investigate potential differences in potency, efficacy and selectivity, while also engaging in covalent binding. Comparative preclinical studies involved pharmacologic profiling in biochemical and functional cellular assays, as well as in a PD model in mice. BTK target occupancy was correlated with PD markers by using a potent and selective biotinylated probe that was developed based on the chemical structure of acalabrutinib. In addition, we aimed to better understand the potential risk of adverse events by investigating the impact of Structure-Reactivity Relationships (SRR) on kinase selectivity. Finally, data are presented on the PK/PD relationships of acalabrutinib in healthy volunteers. The combined features of acalabrutinib result in a selective and potent BTK inhibitor that appears to be differentiated from ibrutinib and spebrutinib, supporting further clinical development.

MATERIAL & METHODS

Biochemical Kinase assays. BTK and ITK enzyme activity was measured using the IMAP (immobilized metal ion affinity-based fluorescence polarization) assay. BTK enzyme (Millipore) or ITK enzyme (Millipore) was diluted to 16 nM and 34 nM, respectively in Kinase Reaction (KR) buffer (10 mM Tris-HCl, 10 mM MgCl2, 0.01% Tween-20, 0.1% NaN3, 1 mM DTT, 2 mM MnCl2, pH 7.5). Serial dilutions log10 from 1 mM to 31.6 nM of test compounds were made in 100% DMSO. The dilutions in DMSO were then diluted 25-fold in KR-buffer. Final compound concentrations ranged from 10 μM to 0.316 nM. 5 μL/well of test compound in KR buffer (final DMSO concentration in the assay is 1%) was mixed with 5 μl/well of BTK or ITK enzyme (final concentration in the assay was 4 and 8 nM for BTK and ITK, respectively). Test compounds and kinase enzyme were pre-incubated 1 hour at room temperature, before adding 5 μL/well of 200 nM Fluorescein labeled substrate peptide (Blk/Lyntide substrate, Molecular Devices) in KR-buffer. Final peptide substrate concentration in assay was 50 nM. The kinase assay was started by adding 5 μL/well of 20 μM ATP in KR-buffer (final ATP concentration was 5 μM ATP, Km ATP). Following incubation for 2 hours at room temperature the enzyme reaction was stopped by adding 40 μL/well IMAP Progressive Binding Solution (Molecular Devices), according to product instructions, using 60% 1x buffer A and 40% 1x buffer B with 800x diluted beads). After a 60-minute incubation at room temperature in the dark the FP signal was read. Fluorescence at 535 nm was measured using parallel and perpendicular filters to determine differences in rotation due to binding of the phosphorylated substrate peptide to the beads. Values were calculated as percentage of the difference in readout (ΔmPi) of the controls with and without ATP. IC_{50} values were determined by curve fitting of the experimental results using Dotmatics.

Inhibitory activity on TEC was measured using the LanthaScreen assay from ThermoFisher according the manufacturer's protocol, using a final concentration of 1 nM of TEC enzyme (LifeTech) and 2 nM Eu-anti-HIS antibody (Invitrogen). Serial dilutions of test compounds were prepared as described above for the BTK and ITK IMAP assays. Test compounds, TEC enzyme/antibody mix and Tracer 178 (Invitrogen, final concentration 1 nM) were mixed and incubated 2 hours at room temperature in the dark, prior to reading the TR-FRET signal at 615 nm and 665 nm. The ratio 665/615 was used to calculate values expressed as

JPET Fast Forward. Published on September 7, 2017 as DOI: 10.1124/jpet.117.242909
This article has not been copyedited and formatted. The final version may differ from this version.

percentage of the difference in readout (S/N) of the controls with and without Tracer. IC_{50} values were determined by curve fitting of the experimental results using Dotmatics. BMX, TXK, EGFR, ErbB2, ErbB4, JAK3, BLK, FGR, FYN, HCK, LCK, LYN, SRC, YES1 kinase activity was measured using the Z'-LYTE assay at Thermo Fisher. A 10-point dose response was generated with 1 hour incubation of the test compound with the kinase prior to initiation of the kinase reaction by the addition of ATP. ATP concentration in the assay was Km ATP for the different kinases. IC_{50} values are determined by curve fitting of the experimental results at Thermo Fisher.

Glutathione Reactivity Assay. 765 μL of a 3.32 mM solution of test compound in methanol was added to 765 μL of a 23.5 mM solution of L-Glutathione reduced (GSH) in phosphate buffer (pH=7.4). The mixtures were stirred in a water bath held at 37°C. At specific time intervals, 200 μL aliquots were taken and analyzed by RP-HPLC (Supplemental). Ln([compound]/[compound]0) was plotted against the time in minutes and linear regression analysis was performed with MS Excel. The time point at which 50% of the compound is consumed via reaction with the GSH (t½) was calculated as: t½ = Ln(2)/k, where k is the negative of the slope of the linear trend line.

Human Blood Collection and Human Peripheral Blood Mononuclear Cell (PBMC) Isolation. Venous blood was collected in heparin tubes from healthy human volunteers and kept at ambient temperature for no longer than 24 hours. In case PBMC were isolated, this was done using the Histopaque gradient purification method (GE Healthcare and cryopreserved in 90% DMSO + 10% FBS).

Inhibition of B cell Receptor (BCR)-induced CD69 Surface Expression in Human B cells. PBMC assay: Cryopreserved PBMC were thawed, washed, and suspended at 2 X 10^5 cells/well in RPMI + 10% FBS in 96-well plates. Test compounds were added to PBMC using a ½ log dose titration (final concentration was 10 μM to 0.316 nM) and incubated for 2h at 37°C, 5% CO_2. Final DMSO concentration in the assay was 0.1%. Goat anti-human IgM F(ab')2 (Southern Biotech) was added and cells were incubated for a further 18 hours. Cells were stained with CD69-FITC, CD19-BV421, and CD3-BV510 antibodies (BD Biosciences) for 30 minutes at 4°C, with 7-AAD as a viability measure, followed by flow cytometry using a FACSVerse flow

JPET Fast Forward. Published on September 7, 2017 as DOI: 10.1124/jpet.117.242909
This article has not been copyedited and formatted. The final version may differ from this version.

cytometer (BD Biosciences). **Whole Blood (WB) assay:** 45 µL blood was diluted 1:1 in RPMI + 1% FBS and incubated with test compound (as described above). Blood was stimulated with 10 µg/mL mouse anti-human anti-IgD (BD Biosciences) and incubation for 18 hours. Cells were stained with CD69-FITC, CD19-BV421, and CD3-BV510 (BD Biosciences) for 15 minutes at room temperature, followed by RBCs lysis with FACS Lysing Solution (BD Biosciences) in a 96-deep well plate. Cells were washed with 1mL/well PBS + 0.5% BSA, pelleted, and resuspended in 200uL/well of PBS + 0.5% BSA, followed by flow cytometry. For both PBMC and WB assays, median fluorescence intensity values for CD69 were obtained from the CD19+ CD3- B lymphocyte gate using FCSExpress analysis software (De Novo Software). EC_{50} values were determined by curve fitting of the experimental results using Dotmatics.

Murine PD model. Balb/c mice were dosed via oral gavage with inhibitors or vehicle and then euthanized after 1 to 24 hours. Extracted spleens were disassociated to obtain single-cell suspensions. Red blood cells (RBC) were lysed with an ammonium chloride solution (Sigma). Remaining cells were washed with cold PBS and counted. An aliquot of 1×10^6 cells was snap frozen (LN_2) as cell pellets for subsequent BTK target occupancy ELISA and the remainder was used for CD69 analysis (see below).

BTK Target Occupancy ELISA. The percent of drug-bound BTK in mouse and human samples was determined by an ELISA based method as follows: OptiPlate 96-well plates (Perkin Elmer) were coated with 125 ng/well anti-BTK Ab (BD Biosciences) and blocked with BSA (Sigma-Aldrich). Samples containing either 5×10^5 or 1×10^6 cells from human PBMC or mouse splenocytes, respectively were lysed in ice cold lysis buffer containing 50 mM Tris-HCl pH 7.5, 250 mM sucrose, 5 mM MgCl2, 1 mM dithiothreitol (DTT), 0.05% digitonin, and protease inhibitor cocktail (Sigma-Aldrich). Cell lysates were then incubated for 1 hour in the absence or presence of 1 µM acalabrutinib, a saturating concentration that results in complete BTK occupancy. The difference with the signal of the cell lysates not incubated with an excess acalabrutinib represents free BTK not occupied by a BTK inhibitor. Samples were incubated for 1 hour with 100 nM biotin tag compound ACP-4016 (**10**). This probe will bind covalently to Cys481 in the ATP pocket in BTK when the ATP pocket is not occupied by a covalent BTK inhibitor. Each sample was then added in duplicate to the prepared Optiplate and incubated for 2 hours at ambient temperature. Plates were washed with PBS + 0.05%

JPET Fast Forward. Published on September 7, 2017 as DOI: 10.1124/jpet.117.242909
This article has not been copyedited and formatted. The final version may differ from this version.

Tween20 four times. Streptavidin-HRP (Invitrogen; ELISA grade) was added at 100 µL/well (120 ng/mL) and incubated for 1 hour at room temperature. Plates were washed with PBS + 0.05% Tween20 three times and then washed with PBS (without Tween 20) two times. One hundred µL/well of SuperSignal ELISA Femto Substrate (ThermoFisher Scientific) was added and then chemiluminescence was measured after 1 minute (EnVision® plate reader; PerkinElmer). The percent of BTK occupancy for each sample time point was calculated relative to the day 1 predose sample for each patient. The signal from the day 1 predose sample without exogenous acalabrutinib represents 100% free BTK (or 0% occupied BTK), whereas the signal from the day 1 predose sample with exogenous acalabrutinib represents 0% free BTK (or 100% occupied BTK). The incubation of each cell lysate with 1 µM acalabrutinib was used to correct for background signal not related to free BTK:

% Free BTK sample X = (Sample X – Sample $X^{+drug[1uM]}$) / (Day 1 Predose – Day 1 $Predose^{+drug[1uM]}$) x 100%

% Occupied BTK = 100% - % Free BTK

Ex Vivo BCR-induced CD69 Expression in Mouse B cells. Splenocytes from drug- and vehicle-treated mice were plated at 2 x 10^5 cells/well in 96-well flat bottom plates. 10 µg/mL goat anti-mouse IgM (Southern Biotech) was added and cultures were incubated for 18 hours in at 37°C, 5% CO_2. Cells were treated with Fc Block (BD Biosciences) and subsequently stained with CD69-FITC, CD19-BV421, CD3-BV510 (BD Biosciences) and 7-AAD, followed by flow cytometry. MFI values for CD69 were obtained from the B lymphocyte gate (CD19+, CD3-). Values were normalized to a percent of control (POC), with the control being the CD69 MFI from the vehicle-treated mice for each time point. Cells without anti-IgM addition served to define the basal expression.

EGF Receptor inhibition. A431 cell line were plated at 4 x 10^4 cells/well in a 96-well culture plate (MicroWell 96-well Microplates, Nunc) in DMEM/HAM F12 + 10% FBS and incubated overnight at 37°C, 5-7% CO_2. Serial dilutions (½ log) of test compounds were made in 100% DMSO and added to the A431 cells (final compound concentration range in the assay from 10 µM to 0.316 nM, final concentration 1% DMSO) and incubated with the cells for 2 hours at 37°C, 5-7% CO_2, followed by a 10-minute stimulation

JPET Fast Forward. Published on September 7, 2017 as DOI: 10.1124/jpet.117.242909
This article has not been copyedited and formatted. The final version may differ from this version.

with EGF (Tebu.bio BV final concentration 250 ng/ml). Culture medium was removed from the cells and 100 µl/well lysis buffer (Cell extraction buffer, Invitrogen + Protease Inhibitor Cocktail, Roche) was added. Cell lysates were used to measure phospho-EGFR ELISA (DuoSet® IC, Human Phospho-EGFR/ErbB1, R&D Systems). EC_{50} values were determined by curve fitting of the experimental results using Dotmatics software.

Jurkat T cell assay. Regulation of anti-CD3/CD28-induced IL-2 production on Jurkat T cells was done using a clone, obtained by dilution cloning, with high expression of IL-2 following stimulation (Jurkat J.E6.2.11). Jurkat cells were plated at $2x10^5$ cells per well in a 96-well culture plate (MicroWell 96-well Microplates, Nunc) cultured in DMEM F12 + 10% FBS and cultured overnight in cell culture incubator, 37%, 5-7% CO_2. Serial dilution (½ log) of test compounds were made in 100% DMSO and added to the Jurkat cells (final compound concentration range in the assay from 10 µM to 0.316 nM, final concentration 0.1% DMSO). Following a 1h incubation the Jurkat cells were stimulated with anti-human CD3 and anti-human CD28 (BD Biosciences, 0.1 µg/ml final concentration in the assay). Cell culture medium was harvested after a 6h incubation following activation and used subsequently to measure IL-2 produced by ELISA (Human IL-2 Cytosets Biosource). EC_{50} values were determined by curve fitting of the experimental results using Dotmatics software.

Human PBMC T cell assay. Cryopreserved PBMC were thawed, washed and suspended at 1 x 10^5 cells/well in RPMI + 10% FBS in 96-well U-bottom polypropylene plates and rested for 1 hour at 37˚C, 5% CO_2. Cells were then pre-treated with a 10-point serial dilution of compounds (as described above for B cell assays). Pre-incubated PBMC were transferred to 96-well round-bottom polystyrene plates that have been coated with anti-human CD3 antibody (Clone UCHT-1, BD Biosciences; coated at 10ug/ml for 2 hours at 37˚C) or uncoated wells for controls and incubated over night at 37˚C, 5% CO_2. PBMC were washed twice in PBS containing 0.5% Bovine serum albumin (PBS + 0.5% BSA) and stained with CD4-AlexaFluor 647 (Clone RPA-T4) and CD8-AlexaFluor 647 (Clone RPA-T8, BD Biosciences), CD19-BV421 (Clone HIB19), CD69-FITC (Clone FN50, BD Biosciences) and CD25-PE-Cy7 antibodies (BD Biosciences) for 30 minutes at 4˚C in the dark. After washing twice in PBS + 0.5% BSA, 7-Aminoactinomycin D (7-AAD, Life Technologies)

JPET Fast Forward. Published on September 7, 2017 as DOI: 10.1124/jpet.117.242909
This article has not been copyedited and formatted. The final version may differ from this version.

was added and cells were analyzed on a FACSVerse flow cytometer (BD Biosciences). The percentages of CD25+ T cells within viable CD4+CD8+CD19- T cells were determined using FCSExpress Software (DeNovo Software, Glendale, CA). EC_{50} values were determined by curve fitting of the experimental results using Dotmatics software.

PK Healthy Volunteers. Acalabrutinib was tested in an escalating dose, safety, and PK/PD study in healthy adult volunteers. Two oral doses of 2.5, 5, 25, 50 mg were administered twelve hours apart on a single day, or administered as a single dose of 75 or 100 mg (Study ACE-HV-001). The study was performed in accordance with the ethical principles stated in the Declaration of Helsinki, US FDA regulation 21 CFR 312, Parts 50 and 56, ICH GCP. All subjects provided informed consent on an IRB-approved protocol. Acalabrutinib was administered after an overnight fast and blood samples were collected for pharmacokinetic (PK) analysis at predose and 15 and 30 minutes, 1, 1.5, 2, 3, 4, 6, 8, 12, 13, 14, 15, 16, 18, 20, 24, 36, 48 and 60 hours postdose (± 5 minutes). Plasma concentrations of acalabrutinib were determined using a validated analytical liquid chromatography-tandem mass spectrometry (LC-MS/MS) method against a stable labeled internal standard at Basi (West Lafayette, IN) in lithium heparin plasma. The quantification range for acalabrutinib was 1-1000 ng/mL.

PK analyses were performed using noncompartmental methods with Phoenix WinNonlin software, (version 6.3, Pharsight Inc., Mountain View, CA) and GraphPad Prism (v 6.00 for Windows, GraphPad Software Inc., La Jolla, CA). The Cmax and Tmax were taken directly from the individual's data. The following PK parameters were derived from the plasma concentrations of acalabrutinib: area under the concentration-time curve (AUC) from time 0 to last quantifiable concentration ($AUC_{0\text{-}last}$); AUC from time 0 to infinity ($AUC_{0\text{-}inf}$); maximum observed plasma concentration (C_{max}); time to reach C_{max} (T_{max}); terminal elimination half-life ($t_{1/2}$); terminal elimination rate constant (λz); The $AUC_{0\text{-}12}$, $AUC_{0\text{-}24}$ and $AUC_{0\text{-}\infty}$ (where data permit) were calculated using the linear trapezoidal method (log / linear rule). As data permit, the elimination rate constant, lambda z (λz), was calculated as the negative of the slope of the terminal log-linear segment of the plasma concentration-time curve. The elimination half-life ($t_{1/2}$) was calculated according to the following equation: $t_{1/2} = 0.693/\lambda z$. Oral clearance (CL/F) and volume of distribution (Vz/F) were calculated according to: $CL/F = (Dose/AUC_{INF})$ and $Vz/F = Dose/\lambda z \bullet AUC_{INF.}$

RESULTS

On Target Biochemical and Functional Characterization and Modeling of BTK Inhibitor Interactions.

Acalabrutinib (**1**) displayed low nanomolar inhibition in the IMAP assay with an IC_{50} value of 5.1 nM. In a head-to-head comparison in the same biochemical assay, ibrutinib (**2)** had a potency (as measured by IC_{50}) of 1.5 nM, while the potency of spebrutinib (**3**) was 2.3 nM (Figure 2). However, the inhibitory potential of spebrutinib was lower in BCR-mediated cell surface expression of CD69 in peripheral blood mononuclear cells (PBMC) and in the human whole blood (hWB) assay. In the latter assay, acalabrutinib (EC_{50} 9.2 ± 4.4 nM) and ibrutinib (EC_{50} 5.8 ± 3.0 nM) showed no statistically significant difference; whereas, spebrutinib was less potent with an EC_{50} of 140 nM. Inversion of the stereochemistry of acalabrutinib had a profound effect on the inhibitory potency of BTK, as demonstrated by the ~130-fold loss in the IMAP assay. The cell-based EC_{50} values of the R-enantiomer (**4**) were consistent with this observation as well, being 592 nM and 1,530 nM in the PBMC and hWB assays, respectively.

Figure 1 shows a model of the acalabrutinib:BTK complex that was created by docking acalabrutinib into the ATP pocket of BTK using a co-crystal structure of a reversible inhibitor:BTK complex (pdb entry 3GEN). The model included minimization of two amino acids residues to accommodate the back pocket filling substituent of acalabrutinib, Met449 and Leu542. This model indicates that H-bonding capabilities of the central 8-aminoimidazopyrazine moiety with Met477 and Glu475 in the hinge region are present. The 2-pyridylbenzamide shows hydrogen bonding interactions with Ser538 and Asp539.

The importance of the 2-pyridyl nitrogen was further elucidated by profiling compounds in which the 2-pyridyl nitrogen is moved to the 3- and 4-position, respectively. Compounds containing 3-pyridyl (**5**) and 4-pyridyl (**6**) moieties were 840- and 360-fold less potent than acalabrutinib in the biochemical assay. Absence of activity was confirmed in peripheral B cells in functional assays using human PBMC and hWB with EC_{50} > 4 μM for both compounds (Figure 2). Data generated on additional compounds highlight the relevance of the positioning of the H-bonding partners when the amide as the linker is employed (Supplemental Table 1). We also explored the impact of (un)substituted acrylamide functions as in compounds **7**, **8** and **9**. Unsubstituted acrylamide compound **7** is generally three-fold more potent in the biochemical and cell-based assays compared with acalabrutinib. However, introduction of a methyl group on the β- (as in **8**) or α-position

JPET Fast Forward. Published on September 7, 2017 as DOI: 10.1124/jpet.117.242909
This article has not been copyedited and formatted. The final version may differ from this version.

(**9**) of the acrylamide reduced the biochemical and cell-based potency by ≥ 100- and ≥ 900-fold, respectively. To demonstrate the relative contribution of affinity and inactivation rate, the K_I and k_{inact} were determined for compounds **1**, **2**, **3** and **7** (Supplemental Table 2). The higher potency of acrylamide compound **7** compared to acalabrutinib seems to depend primarily on a faster inactivation rate (k_{inact}) as the affinity (K_I) was relatively similar. For ibrutinib, the affinity component appears to be a relative important contributor to the observed potency.

Glutathione Thiol Reactivity and Kinase Selectivity. Since the microenvironment of Cys481 in BTK has been reported to augment the nucleophilicity of the cysteine compared with some other cysteine-containing kinases, it presents an opportunity to improve (ie, reduce) the electrophilicity of covalent binding BTK inhibitors. The pK_a of the cysteine sulfhydryl group is directly influenced by proximal amino acids (Kortemme and Creighton, 1995; Garske et al., 2011). All TEC kinases – except ITK – contain an asparagine (Asn) residue at the i+3 position with respect to the reactive cysteine, and this results in a reported pK_a of approximately 7.7 for Cys481 in BTK (Zapf et al., 2012). Intriguingly, the other cysteine-containing kinases such as EGFR, ERBB2, BLK and JAK3 have an aspartate (Asp) in this position, which has been suggested to increase the pK_a, and thus lower the nucleophilicity of the sulfhydryl group. Current data suggest that the thiol pK_a increases by about 0.6 – 1.3 log units for the Asp containing kinases (Supplemental Table 3). Lower intrinsic electrophilicity of a covalent inhibitor appears to reduce the likelihood of covalent binding to off-target cysteines with a lower nucleophilicity, and favorably affect kinase selectivity within the kinase subset with an Asp in the i+3 position while preserving potency for BTK.

To further substantiate whether the relative reactivity of the electrophilic moieties could impact the BTK potency and the overall kinase selectivity profile, the inhibitors were reacted with glutathione (GSH) in a semi-physiological setting. Acalabrutinib has a butynamide moiety, which contributes to a slower conversion of the parent with a half-life ($t_{1/2}$) of 5.5 hours (Figure 2). In contrast, the acrylamide containing compounds ibrutinib and spebrutinib were more rapidly consumed than acalabrutinib, with average $t_{1/2}$ values of 2 hours and 1 hour, respectively. Intriguingly, compound **7** displayed a much faster turn over than acrylamides ibrutinib and spebrutinib. The closer proximity of the electrophile in **7** to the electron-deficient central heteroaryl imidazopyrazine moiety could augment the electrophilicity, and may explain the lower t½ average

JPET Fast Forward. Published on September 7, 2017 as DOI: 10.1124/jpet.117.242909
This article has not been copyedited and formatted. The final version may differ from this version.

of 0.6 hour. Methyl compounds **8** and **9** lose the capacity to react with GSH, which suggests that the degree of BTK inhibition observed could be due to reversible binding (Figure 2). The observation that compound **8** still displayed some residual activity suggests that steric hindrance in proximity of Cys481 impacts the binding potential, rather than the relative electrophilicity of the reactive group per se.

Profiling of the clinical BTK inhibitors and compound **7** on the cysteine kinase panel, distinguishes acalabrutinib from the acrylamide compounds in terms of selectivity. All kinases with an Asp in the i+3 position were not sensitive to acalabrutinib, and the inhibition of TEC, BMX and TXK kinases was lower than for any of the acrylamide compounds. A direct comparison of the IC_{50} values of acalabrutinib and acrylamide containing compound **7**, revealed the influence of the warhead choice on the cysteine-kinase selectivity profile (Table 2). In this data set, ERBB4 is an outlier, as this is the only kinase that has a glutamate (Glu) in the i+3 position. While the predicted cysteine pK_a is at par with Asp kinases, the tested compounds acalabrutinib, ibrutinib, spebrutinib and acrylamide **7** all displayed single or double digit nM inhibition in the biochemical assay for ERBB4. Since spebrutinib was the most reactive, yet the least potent on ERBB4 (IC_{50} = 49 nM), the inhibition of ERBB4 may be governed to a lesser extent by the electrophilic nature of the reactive moiety. Each of the clinical BTK inhibitors were also profiled at 1 μM in a competition binding assay on a panel of 456 human kinases (KINOME scan at DiscoveRx). Of these kinases, 395 are non-mutant protein kinases. Our results demonstrate that acalabrutinib is the most selective BTK inhibitor of the three compounds profiled (Figure 3). For acalabrutinib, only 1.5% of the non-mutant protein kinases were inhibited ≥65% at 1 μM. For ibrutinib and spebrutinib, 8.9% and 7.6%, respectively, of the non-mutant protein kinases were inhibited ≥65% at 1 μM. Interestingly, strong inhibition by ibrutinib was observed for all kinases belonging to the SRC-family kinases, which is in line with earlier published results (Honigberg et al., 2010) and our own data (Byrd et al., 2016). Spebrutinib showed a more scattered inhibition over the kinase phylogenetic tree. Evaluation of SRC-family kinase inhibition confirmed that acalabrutinib did not inhibit any member (IC_{50} values all exceeding 1 μM); whereas, ibrutinib demonstrated single- or double-digit nanomolar inhibition on all members tested (Supplemental Table 4).

Off-target cellular activities of BTK inhibitors. The functional relevance of the differences in the observed biochemical inhibition of non-BTK kinases by acalabrutinib, ibrutinib, spebrutinib and compound **7** was

JPET Fast Forward. Published on September 7, 2017 as DOI: 10.1124/jpet.117.242909
This article has not been copyedited and formatted. The final version may differ from this version.

explored in specific cell lines. EGFR inhibition of selected BTK inhibitors was tested in two EGFR expressing human tumor cells lines: An epidermoid carcinoma (A431) cell line (Table 3) and a bladder carcinoma (HT-1376) cell line (Supplemental Figure 1). Both cell lines gave similar EC_{50} values for the tested compounds on EGF-induced EGFR phosphorylation. Acalabrutinib showed no or only minimal inhibition up to a concentration of 10 µM. Results with compound **7** suggest that this is due to the electrophile switch from acrylamide to butynamide. Spebrutinib inhibited EGF-induced EGFR phosphorylation with an EC_{50} of 4.7 µM, which suggests that the reactivity of electrophile is not the only parameter relevant for kinase selectivity. Ibrutinib inhibited EGF-induced EGFR phosphorylation in A431 cells with an EC_{50} value of 71 nM.

The compounds were also evaluated in T cell functional assays. First, the compounds were profiled in anti-CD3/CD28-induced IL-2 production in Jurkat T cells, using a Jurkat E6 T cell clone with high IL-2 expression following stimulation. Ibrutinib and spebrutinib showed inhibition of anti-CD3/anti-CD28-induced IL-2 production with an EC_{50} of 99 and 150 nM, respectively (Table 3). Also, in line with the biochemical data on ITK, compound **7** was less potent in the Jurkat T cell assay than ibrutinib and spebrutinib. Acalabrutinib displayed an EC_{50} > 10 µM in the Jurkat T cell assay, which is expected given its biochemical selectivity over T cell kinases ITK and TXK. In addition, effects in PBMC were studied by measuring the inhibition of anti-CD3-induced CD25 cell surface expression on human peripheral T cells. The order of inhibitory potential of the tested compounds followed the ranking as determined in Jurkat cells, with ibrutinib being the most potent (EC_{50} = 257 nM) and acalabrutinib being the least potent (EC_{50} > 10 µM) (Table 3).

Preclinical PD model in mice. To investigate potency in vivo, mice were treated with oral doses ranging from 0.1 – 30 mg/kg of acalabrutinib, ibrutinib, spebrutinib, or with vehicle. Three hours after dosing, spleens were extracted and single cell suspensions of splenocytes were prepared. The splenocytes were stimulated with anti-IgM for 18h, followed by analysis of CD69 expression by flow cytometry gated on CD19+ B cells (Figure 4). ED_{50} determinations showed that acalabrutinib was the most potent BTK inhibitor in vivo (1.3 mg/kg), followed by ibrutinib (2.9 mg/kg), and spebrutinib (20 mg/kg). Due to the covalent nature of binding, BTK inhibitors have been shown to have a prolonged PD effect even as plasma drug levels fall to undetectable levels. To investigate this, a return of function (ROF) experiment was performed investigating anti-IgM-

JPET Fast Forward. Published on September 7, 2017 as DOI: 10.1124/jpet.117.242909
This article has not been copyedited and formatted. The final version may differ from this version.

induced CD69 expression on the splenocyte B cells and BTK target occupancy in the splenocytes. The potent biotinylated probe ACP-4016 (**10**) was developed to support development of an ELISA-based BTK target occupancy assay (Figure 4D). The biochemical IC_{50} value of the probe averaged 2.2 nM (Supplemental Table 1). Mice (five per group) were dosed orally with a single dose of acalabrutinib, ibrutinib, spebrutinib (25 mg/kg) or vehicle. Spleens were extracted 3, 6, 12, 18 or 24h after dosing and single cell suspensions were prepared. Splenocytes were cultured and stimulated with anti-IgM for 18h, followed by CD69 surface expression measurement (Figure 4B), or used directly in the BTK target occupancy assay (Figure 4C). Acalabrutinib and ibrutinib showed (near) complete BTK occupancy along with complete inhibition of anti-IgM-induced CD69 expression on splenocyte B cells for the 3h post-dose time point. These results are in line with the dose response data showing full inhibition of splenocyte B cells at oral doses ≥ 10 mg/kg for acalabrutinib and ibrutinib, 3h after dosing. Additional experiments demonstrated that complete BTK target occupancy and full B cell de-activation is already achieved 1h after dosing (data not shown). In contrast, a 25-mg/kg dose of spebrutinib showed incomplete BTK target occupancy (~15% free BTK versus vehicle control) and inhibition of anti-IgM-induced CD69 expression on peripheral B cells (~25% remaining activity versus vehicle control). This again corresponded with the observed higher ED_{50} of 20 mg/kg for this BTK inhibitor. Over time, an increase in the amount of free BTK and an increase in splenocyte B cell function is demonstrated, as measured by function of anti-IgM-induced CD69 expression. However, BTK target occupancy and inhibition of B cell function was still observed 24 hours post-dose. Acalabrutinib and ibrutinib displayed around 35% free BTK and 40% B cell activity versus vehicle control at 24 hours post-dose, whereas for spebrutinib, ~55% free BTK and 75% splenocyte B cell activity was observed at this time point. The average return rate for all three BTK inhibitors was estimated using linear fitting of the data for the return of B cell function (anti-IgM-induced CD69 expression on splenocyte B cells) and the return of free BTK. These return rates were 2.0 ± 0.2% and 1.7 ± 0.1% per hour, respectively.

PK/PD Healthy Volunteers. PK properties and safety of acalabrutinib were evaluated in a sequential dose-escalation study in healthy adult volunteers (six per group) after oral administration of two doses of 2.5, 5, 25, or 50 mg given twelve hours apart on a single day and a single dose of either 75 or 100 mg. Acalabrutinib was rapidly absorbed with median time to maximum plasma concentration (T_{max}) values between 0.5 and 1.0

hour for all dose cohorts, independent of dose level (Supplemental Figure 2, Supplemental Table 5). The increase in mean C_{max} was greater than dose proportional from 5 to 25 mg. However, between 2.5 to 5.0 mg, 25 to 50 mg, and 50 mg to 100 mg, the increases in mean C_{max} were close to dose proportional. The mean values AUC_{0-12}, AUC_{0-24} or AUC_{0-inf}, increased in a dose proportional manner based on the increases of the total dose administered (Figure 5A). Linear regression analysis of the natural log (ln) transformed AUC_{0-24} and AUC_{0-inf} relative to the ln transformed dose administered, indicated that the increases in AUC relative to the increases in dose administered were linear. Rapid elimination was observed with mean half-life ($t_{1/2}$) values ranging from 0.88 hour to 2.1 hours in Cohort 1 to 5. The mean calculated CL/F values ranged from 165 to 219 L/h and appeared to be independent of the dose administered. The Vz/F values ranged from 233 to 612 L and also appeared to be independent of the dose administered.

Sixteen of 59 (27%) enrolled subjects reported one or more adverse events on study. All adverse events were Grade 1 or Grade 2. No serious adverse events occurred on the study. Of the adverse events reported, 3 events (constipation, somnolence and feeling cold) were assessed as related to acalabrutinib. No study-drug related adverse events lead to discontinuation from the study. No effect of acalabrutinib was observed on any laboratory parameters (ie, hematology, serum chemistry, urinalysis, cardiac troponin I and C reactive protein). No effect was observed of acalabrutinib on physical exams, vital signs or ECG parameters.

The pharmacodynamics of acalabrutinib was evaluated using the BTK occupancy assay and measuring the inhibition of CD69 expression on B cells after ex vivo BCR-stimulation. Both PD readouts were dose-dependent, with a plateau observed at the 75- and 100-mg dose levels, 3 hours after acalabrutinib administration. At this timepoint, the degree of BTK median occupancy was around 99% for the 75- and 100-mg dose (Figure 5B). This correlated with near complete inhibition for CD69 (Figure 5C) for the same doses and time point. However, only the 100-mg cohort maintained high BTK median occupancy and high BCR functional inhibition over time (Figure 5D). At 12 hours, the median occupancy was 99% and median CD69 inhibition was 95%, whereas at 24 hours these parameters were 90% and 84%, respectively. CD86 expression levels were also determined in parallel and essentially matched the inhibition of CD69 expression (data not shown).

DISCUSSION

Acalabrutinib was identified as a BTK inhibitor with a differentiated kinase selectivity profile compared to other BTK inhibitors in development. Key structural components of acalabrutinib include a 2-pyridylbenzamide moiety, and the electrophilic 2-butynamide moiety that is involved in covalent binding to Cys481. The proximal positioning of the 2-butynamide moiety to the electron-deficient (and thus electron-withdrawing) imidazopyrazine core may help to re-activate this otherwise fairly inert functionality. The potency difference of the enantiomeric pair (compare acalabrutinib and **4**) showed that the activity primarily resides in the S-enantiomer, suggesting better positioning of the butynamide moiety. As demonstrated in the GSH assay, acalabrutinib displayed lower reactivity than acrylamides ibrutinib, spebrutinib and compound **7**. This may help to minimize inhibition of cysteine kinases that exhibit higher cysteine pK_a values equivalent to Cys481 in BTK. Indeed, acalabrutinib is the most selective with regards to inhibition of TEC-, EGFR- and SRC-family kinases. The correlation of biochemical off-target inhibition and functional consequences in selected cell lines was confirmed for different kinases.

Inhibitors of the EGFR signaling pathway cause skin rash and diarrhea, and these toxicities are believed to be “class effects” (Lynch et al., 2007; Dy and Adjei, 2013). With respect to the inhibitory potential for EGFR, the rank order of compounds was identical in biochemical and cellular settings, acalabrutinib showing a lack of functional inhibitory effects (EC_{50} >10 µM). The events of diarrhea reported during acalabrutinib treatment of CLL patients (38% grades 1-2, 39% all grades) have been generally mild (Byrd et al., 2016). Given the observed exposure levels of acalabrutinib following a single oral dose of 100 mg (580 ± 150 ng/mL), and the absence of effects on pEGFR inhibition in two relevant cell lines at these concentrations, we do not expect to see EGFR-mediated adverse events for acalabrutinib.

ITK signaling in Jurkat cells and in primary human peripheral T cells correlated with the biochemical IMAP data. The drug concentrations needed to inhibit IL-2 production in Jurkat cells and modulation of human peripheral T cells may well be achieved in patients treated with ibrutinib or spebrutinib (Dubovsky et al., 2013; Evans et al., 2013), and therefore may bear physiological relevance. Indeed, ibrutinib is a reported irreversible covalent ITK inhibitor with confirmed occupancy on this kinase in CLL patients (Dubovsky et al., 2013). Treatment with ibrutinib reduced the number of Th17 T cells as a percentage of the total T cell

JPET Fast Forward. Published on September 7, 2017 as DOI: 10.1124/jpet.117.242909
This article has not been copyedited and formatted. The final version may differ from this version.

population in CLL patients, as well as Th17 development from mouse naïve CD4+ T cells. The mouse observations are in line with data reported for ITK -/- mice, in which a shift in the balance from Th17 to Tregs was observed (Gomez-Rodriguez et al., 2014). The same authors reported that this effect is even more pronounced in ITK/TXK -/- mice (Gomez-Rodriguez et al., 2011), indicating redundancy between ITK and TXK. Since ibrutinib inhibits both ITK and TXK in the low nM range in the biochemical assays, the effects of ibrutinib on T cell differentiation most likely mimic the double knockout phenotype. ITK is also expressed in NK cells, and inhibition thereof has been reported to decrease the antibody-dependent cellular cytotoxicity (ADCC) function of NK cells (Khurana et al., 2007). It was reported that ibrutinib inhibited both rituximab- and trastuzumab-induced NK cell cytokine secretion and lysis in vitro in a dose-dependent manner (0.1 and 1 μM), while acalabrutinib did not show any effects at 1 μM (Rajasekaran et al., 2014). This indicates that acalabrutinib is associated with a reduced risk of affecting ADCC-mediated therapies.

An increased incidence in severe hemorrhage was reported in patients treated with ibrutinib, and has been attributed to the effect of ibrutinib on several distinct signaling pathways (Byrd et al., 2015; Shatzel et al., 2017; Wang et al., 2015). Therefore, patients receiving ibrutinib are monitored to reduce the potential of bleeding risk. While the role of BTK on collagen-induced platelet aggregation has been well described, there is no general increase of bleeding risk in XLA patients lacking functional BTK (Quek et al., 1998; Winkelstein et al., 2006), suggesting that BTK inhibition alone is likely not responsible for increased bleeding risk. In platelets, the downstream signaling of several receptors on platelets, including the platelet collagen receptor glycoprotein VI (GPVI) and C-type lectin-like receptor 2 (CLEC-2), is mediated by BTK and TEC (Shatzel et al., 2017). Earlier, we reported on differences in platelet aggregation using platelets from patients treated with acalabrutinib or ibrutinib (Byrd et al., 2016). In an in vivo thrombus formation model, diminished platelet reactivity was observed in samples from patients treated with ibrutinib, while platelets from acalabrutinib-treated patients showed similar reactivity to those derived from non-treated, healthy controls. As TEC kinase phosphorylation is highly dependent on platelet aggregation (Atkinson et al., 2003; Hamazaki et al., 1998), the level of TEC inhibition may govern the bleeding risk. The relative biochemical IC_{50} values for TEC of acalabrutinib (126 nM) and ibrutinib (10 nM) may well contribute to the observed differences in the above model. In addition, inhibition of SRC family kinases by ibrutinib may also play a role in the observed bleeding incidence in ibrutinib-treated patients through modulation of fibrinogen- and von

Willebrand factor-induced platelet activation (Séverin et al., 2012; Senis et al., 2014). Even though inhibition of these kinases by ibrutinib is reversible of nature, modulation of SRC-mediated platelet activation may be anticipated at exposure levels observed in ibrutinib-treated patients. For instance, it has been reported that ibrutinib demonstrated potent inhibition of phosphorylation of SRC-family members LCK and SRC in T cells, with an EC_{50} of less than 0.2 μM, whereas the EC_{50} for acalabrutinib was not reached at 10 μM (Patel et al., in press). Again, these data correspond well with the nanomolar inhibition by ibrutinib for both SRC and LCK. Taken together, these observations indicate that effects of ibrutinib on bleeding could be multifactorial. The improved selectivity profile of acalabrutinib for BTK versus TEC and certain SRC-family kinases may prove advantageous in this regard.

Overall, the biochemical potency of all compounds tested for BTK activity traced well with the inhibitory potential of marker CD69 in our PBMC and hWB assays, except for spebrutinib. For instance, the potency of BTK-mediated inhibition of peripheral B cell function in hWB was approximately 15-fold lower for spebrutinib than for acalabrutinib and ibrutinib. This suggests that plasma proteins or other components of hWB (eg, red blood cells, platelets or neutrophils) may contribute to a lower free fraction of spebrutinib that is available for BTK inhibition. The in vivo potency data generated in the mouse PD model mirrored the cellular data generated, except that acalabrutinib showed better potency than ibrutinib in vivo. With spebrutinib, efficacy could be obtained at higher dosages, but potency was inferior to acalabrutinib and ibrutinib. Evaluation of return of free BTK and return of B cell function in mice, demonstrated that the return rate is independent of the type of BTK inhibitor tested. Hence, the de novo synthesis rate of BTK is the primary driver for the loss of PD effect in a single dose setting.

In human healthy subjects, acalabrutinib is an orally bioavailable BTK inhibitor with fast absorption, dose-proportional PK, and a short half-life in systemic circulation. Despite the short half-life, acalabrutinib had a pronounced on-target impact in peripheral blood B cells that was dose-dependent. Complete BTK occupancy was observed 3 and 12 hours after a single 100-mg dose indicating a saturating concentration was achieved that resulted in near-complete inhibition of a BCR-induced functional response (ie, CD69 expression). Both measures remained high for 24 hours. Therefore, covalent modification of BTK by acalabrutinib prolonged target occupancy and PD that extend beyond the relatively short plasma-half-life in healthy volunteers. In patient populations with more rapidly proliferating B cells, we anticipate an increased de novo synthesis rate

of BTK, suggesting that more frequent dosing may be required to achieve optimal BTK inhibition. Indeed, a 100-mg BID dose in CLL patients showed a higher median BTK occupancy, with less variability at trough, than the 100-mg and 250-mg QD cohorts (Byrd et al., 2016). This illustrates that maximal target coverage can be achieved with BID dosing, which we believe is advantageous for optimal treatment across B-cell malignancy patient populations.

In conclusion, monitoring SRR may help to mitigate the risk for off-target adverse events related to reactivity of the electrophile (Barf and Kaptein, 2012). Low electrophilicity is an important feature to consider to progress the most suitable covalent inhibitor candidates through the pipeline. The use of a straightforward GSH assay to assess the likelihood and the kinetics of covalent binding has revealed a difference in reactivity between compounds containing butynamide and acrylamide moieties. We believe that the lower electrophilicity of acalabrutinib along with higher nucleophilicity of Cys481 in BTK contributes to the observed selectivity profile, which may reduce off-target mediated adverse events. In combination with the improved in vivo potency, acalabrutinib appears to have a differentiated pre-clinical profile from ibrutinib and spebrutinib. Selective covalent BTK probe **10** helped to confirm the correlation of the degree of BTK occupancy and engagement by acalabrutinib in preclinical and clinical settings. Acalabrutinib is a rapidly absorbed covalent BTK inhibitor with a short half-life, yet reaches full target occupancy at a single oral dose of 100 mg in healthy human subjects. Clinical evaluation of acalabrutinib in multiple B-cell malignancies, solid tumors and selected autoimmune indications is currently in progress.

ACKNOWLEDGMENTS

We thank Anouk de Jong for performing the PBMC T cell assays, Tim Ingallinera for preparing the in vivo formulations for the mouse PD experiments, Gerjan de Bruin for analysis of the K_I and k_{inact} data, and Greg Slatter for the discussion on the human PK/PD data. BioAxis Research BV is acknowledged for the pK_a modeling of kinase cysteines. Final versions of the figures were created by Cognition Studios.

AUTHORSHIP CONTRIBUTIONS

Participated in research design: Barf, Covey, Izumi, Gulrajani, Mittag, Pearson, Ulrich and Kaptein

Conducted experiments: Barf, van de Kar, Gulrajani, van Lith, van Hoek, de Zwart, Mittag, Demont, Verkaik, Krantz

Performed data analysis: Barf, Covey, Izumi, van de Kar, Gulrajani, van Lith, van Hoek, de Zwart, Mittag, Demont, Verkaik, Krantz, Pearson, and Kaptein

Wrote or contributed to the writing of the manuscript: Barf, Covey, Izumi, Pearson, and Kaptein.

REFERENCES

Atkinson BT, Ellmeijer W, and Watson SP (2003) Tec regulates platelet activation by GPVI in the absence of Btk *Blood* **102**: 3592–3599.

Barf T and Kaptein A (2012) Irreversible protein kinase inhibitors: Balancing the benefits and risks *J Med Chem* **55**: 6243–6262.

Bender AT, Pereira A, Fu K, Samy E, Wu Y, Liu-Bujalski L, Caldwell R, Chen Y-Y, Tian H, Morandi F, Head J, Koehler U, Genest M, Okitsu SL, Xu D, and Grenningloh R (2016) Btk inhibition treats TLR7/IFN driven murine lupus *Clin Immunol* **164**: 65–77.

Brown JR, Harb WA, Hill BT, Gabrilove J, Sharman JP, Schreeder MT, Barr PM, Foran JM, Miller TP, Burger JA, Kelly KR, Mahadevan D, Ma S, Li Y, Pierce DW, Barnett E, Marine J, Miranda M, Azaryan A, Yu X, Nava-Parada P, Mei J, and Kipps TJ (2016) Phase I study of single-agent CC-292, a highly selective Bruton's tyrosine kinase inhibitor, in relapsed/refractory chronic lymphocytic leukemia *Haematologica* **101**: e295–298.

Byrd JC, O'Brien S, and James DF (2013) Ibrutinib in relapsed chronic lymphocytic leukemia. *N Engl J Med* **369**: 1278–1279.

Byrd JC, Furman RR, Coutre SE, Burger JA, Blum KA, Coleman M, Wierda WG, Jones JA, Zhao W, Heerema NA, Johnson JA, Shaw Y, Bilotti E, Zhou C, James DF, and O'Brien S (2015) Three-year follow-up of treatment-naïve and previously treated patients with CLL and SLL receiving single-agent ibrutinib *Blood* **125**: 2497–2506.

Byrd JC, Harrington, B, O'Brien S, Jones JA, Schuh A, Devereux S, Chaves J, Wierda WG, Awan FT, Brown, JR Hillmen P, Stephens DM, Ghia P, Barrientos JC, Pagel JM, Woyach J, Johnson D, Huang J, Wang X, Kaptein A, Lannutti, BJ, Covey T, Fardis M, McGreivy J, Hamdy A, Rothbaum W, Izumi R, Diacovo TG, Johnson AJ, and Furman RR (2016) Acalabrutinib (ACP-196) in Relapsed Chronic Lymphocytic Leukemia. *N Engl J Med* **374**: 323–332.

de Weers M, Verschuren MC, Kraakman ME, Mensink RG, Schuurman RK, van Dongen JJ, and Hendriks RW (1993) The Bruton's tyrosine kinase gene is expressed throughout B-cell differentiation, from early

precursor B-cell stages preceding immunoglobulin gene rearrangement up to mature B-cell stages *Eur J Immunol* **23**: 3109–3114.

Dubovsky JA, Beckwith KA, Natarajan G, Woyach JA, Jaglowski S, Zhong Y, Hessler JD, Liu T-M, Chang BY, Larkin KM, Stefanovski MR, Chappell DL, Frissora FW, Smith LL, Smucker KA, Flynn JM, Jones JA, Andritsos LA, Maddocks K, Lehman AM, Furman R, Sharman J, Mishra A, Caligiuri MA, Satoskar AR, Buggy JJ, Muthusamy N, Johnson AJ, and Byrd JC (2013) Ibrutinib is an irreversible molecular inhibitor of ITK driving a Th1-selective pressure in T lymphocytes *Blood* **122**: 2539–2549.

Dy GK and Adjei AA (2013) Understanding, recognizing, and managing toxicities of targeted anticancer therapies *CA Cancer J Clin* **63**: 249–279.

Ellmeier W, Abramova A, and Schebesta A (2011) Tec family kinases: regulation of FcεRI-mediated mast cell activation *FEBS J* **278**: 1990–2000.

Evans EK, Tester R, Aslanian S, Karp R, Sheets M, Labenski MT, Witowski SR, Lounsbury H, Chaturvedi P, Mazdiyasni H, Zhu Z, Nacht M, Freed MI, Petter RC, Dubrovskiy A, Singh J, and Westlin WF (2013) Inhibition of Btk with CC-292 provides early pharmacodynamic assessment of activity in mice and humans *J Pharmcol Exp Ther* **346**: 219–228.

Garske AL, Peters U, Cortesi AT, Perez JL, and Shokat KM (2011) Chemical genetic strategy for targeting protein kinases based on covalent complementarity *Proc Natl Acad Sci USA* **108**: 15046–15052.

Gomez-Rodriguez J, Kraus ZJ, and Schwartzberg PL (2011) Tec family kinases Itk and Rlk / Txk in T lymphocytes: cross-regulation of cytokine production and T-cell fates *FEBS Journal* **278**: 1980–1989.

Gomez-Rodriguez J, Wohlfert EA, Handon R, Meylan F, Wu JZ, Anderson, SM, Kirby MR, Belkaid, Y, and Schwartzberg PL (2014) Itk-mediated integration of T cell receptor and cytokine signaling regulates the balance between Th17 and regulatory T cells *J Exp Med* **211**: 529–543.

Grenningloh R (2016) Discovery of the highly specific BTK inhibitor M2951 and Pharmacodynamic Modeling of BTK Occupancy versus Efficacy in RA and SLE models *14th Annual Discovery on Target, Boston (MA).*

Hamazaki Y, Kojima H, Mano H, Nagata Y, Todokoro K, Abe T, and Nagasawa T (1998) Tec is involved in G protein-coupled receptor-and integrin-mediated signaling in human blood platelets *Oncogene* **16**: 2773–2779.

Hendriks RW, Yuvaraj S, and Kil LP (2014) Targeting Bruton's tyrosine kinase in B-cell malignancies *Nat Rev Cancer* **14**: 219–232.

Herman SEM, Montraveta A, Niemann CU, Mora-Jensen H, Gulrajani M, Krantz F, Mantel R, Smith LL, McClanahan F, Harrington BK, Colomer D, Covey T, Byrd JC, Izumi R, Kaptein A, Ulrich R, Johnson AJ, Lannutti BJ, Wiestner A, and Woyach JA (2016) The Bruton Tyrosine Kinase (BTK) Inhibitor Acalabrutinib Demonstrates Potent On-Target Effects and Efficacy in Two Mouse Models of Chronic Lymphocytic Leukemia *Clin Cancer Res* doi: 10.1158/1078-0432.CCR-16-0463.

Honigberg L, Smith AM, Sirisawad M, Verner E, Loury D, Chang B, Li S, Pan Z, Thamm DH, Miller RA, and Buggy JJ (2010) The Bruton tyrosine kinase inhibitor PCI-32765 blocks B-cell activation and is efficacious in models of autoimmune disease and B-cell malignancy *Proc Natl Acad Sci USA* **107**: 13075–13080.

Jongstra-Bilen J, Puig Cano A, Hasija M, Xiao H, Smith CI, and Cybulsky MI.(2008) Dual functions of Bruton's tyrosine kinase and Tec kinase during Fcgamma receptor-induced signaling and phagocytosis *J Immunol* **181**: 288–298.

Katz FE, Lovering RC, Bradley LA, Rigley KP, Brown D, Cotter F, Chessells JM, Levinsky RJ, and Kinnon C (1994) Expression of the X‐linked agammaglobulinemia gene, btk in B-cell acute lymphoblastic leukemia *Leukemia* **8**: 574–577.

Khurana D, Arneson, LN, Schoon, RA, Dick, CJ, and Leibson PJ (2007) Differential regulation of human NK cell-mediated cytotoxicity by the tyrosine kinase Itk *J Immunol* **178**: 3575–3582.

Kortemme T and Creighton TE (1995) Ionisation of cysteine residues at the termini of model alpha-helical peptides. Relevance to unusual thiol pK_a values in proteins of the thioredoxin family *J Mol Biol* **253**: 799−812.

Lynch TJ Jr, Kim ES, Eaby B, Garey J, West DP, and Lacouture ME (2007) Epidermal growth factor receptor inhibitor-associated cutaneous toxicities: an evolving paradigm in clinical management *Oncologist* **12**: 610–621.

Norman P (2016) Investigational Bruton's tyrosine kinase inhibitors for the treatment of rheumatoid arthritis *Exp Opin Invest Drugs* **25**: 891–899.

O'Brien S, Furman RR, Coutre SE, Sharman JP, Burger JA, Blum KA, Grant B, Richards DA, Coleman M, Wierda WG, Jones JA, Zhao W, Heerema NA, Johnson AJ, Izumi R, Hamdy A, Chang BY, Graef T, Clow F, Buggy JJ, James DF, Byrd JC (2014) Ibrutinib as initial therapy for elderly patients with chronic lymphocytic leukaemia or small lymphocytic lymphoma: an open-label, multicenter phase 1b/2 trial *Lancet Oncol* **15**: 48–58.

Pan Z, Scheerens H, Li S-J, Schultz BE, Sprengeler PA Burrill LC, Mendonca RV, Sweeney MD, Scott KCK, Grothaus PG, Jeffery DA, Spoerke JM, Honigberg LA, Young PR, Dalrymple SA, and Palmer JT (2007) Discovery of selective irreversible inhibitors for Bruton's Tyrosine Kinase *ChemMedChem* **2**: 58–61.

Park JK, Byun J-Y, Park JA, Kim Y-Y, Lee YJ, Oh JI, Jang SY, Kim YH, Song YW, Son J, Suh KH, Lee Y-M, and Lee EB (2016) HM71224, a novel Bruton's tyrosine kinase inhibitor, suppresses B cell and monocyte activation and ameliorates arthritis in a mouse model: a potential drug for rheumatoid arthritis *Arthritis Res Ther* **18**: 1–9.

Patel V, Balakrishnan K, Bibikova E, Ayres M, Keating MJ, Wierda WG, and Gandhi V (2016) Comparison of acalabrutinib, a selective Bruton tyrosine kinase inhibitor, with ibrutinib in chronic lymphocytic leukemia cells *Clin Cancer Res* doi: 10.1158/1078-0432.CCR-16-1446.

Ponader S and Burger JA (2014) Bruton's Tyrosine Kinase: From X-Linked Agammaglobulinemia Toward Targeted Therapy for B-Cell Malignancies *J Clin Oncol* **32**: 1830–9.

Quek LS, Bolen J, and Watson SP (1998) A role for Bruton's tyrosine kinase (Btk) in platelet activation by collagen *Curr Biol* **8**:1137–1140.

Rajasekaran N, Sadaram M, Hebb J, Sagiv-Barfi I, Ambulkar S, Rajapaksa A, Chang S, Chester C, Waller E, Wang L, Lannutti B, Johnson D, Levy R, and Kohrt HE (2014) Three BTK-Specific Inhibitors, in Contrast to Ibrutinib, Do Not Antagonize Rituximab-Dependent NK-Cell Mediated Cytotoxicity *Blood* **124**: 3118.

Senis YA, Mazharian A, and Mori J (2014) Src family kinases: at the forefront of platelet activation *Blood* **124**: 2013–2024.

Séverin S, Nash CA, Mori J, Zhao Y, Abram C, Lowell CA, Senis YA, and Watson SP (2012) Distinct and overlapping functional roles of Src family kinases in mouse platelets *J Thromb Haemost* **10**: 1631–1645.

Shatzel JJ, Olson SR, Tao DL, McCarty OJT, Danilov AV, and DeLoughery TG (2017) Ibrutinib-associated bleeding: pathogenesis, management, and risk reduction strategies *J Thromb Haemost* **15**: 835–847.

Smith PF, Krishnarajah J, Nunn PA, Hill RJ, Karr D, Tam D, Masjedizadeh M, and Gourlay SG (2015) A phase 1 clinical trial of PRN1008, an oral, reversible, covalent BTK inhibitor demonstrates clinical safety and therapeutic levels of BTK occupancy without sustained systemic exposure *EULAR* Abstract SAT0232.

Tam C, Grigg AP, Opat S, Ku M, Gilberson M, Anderson MA, Seymour JF, Ritchie DS, Dicorleto C, Dimovski B, Hedrick E, Yang J, Wang L, Luo L, Xue L, and Roberts AW (2015) The BTK Inhibitor, Bgb-3111, Is Safe, Tolerable, and Highly Active in Patients with Relapsed/ Refractory B-Cell Malignancies: Initial Report of a Phase 1 First-in-Human Trial *ASH 57th Annual Meeting & Exposition, Orlando (FL)* Abstract 832.

Walter HS, Rule SA, Dyer MJS, Karlin L, Jones C, Cazin B, Quittet P, Shah N, Hutchinson CV, Honda H, Duffy K, Birkett J, Jamieson V, Courtenay-Luck N, Yoshizawa T, Sharpe J, Ohno T, Abe S, Nishimura A, Cartron G, Morschhauser F, Fegan C, and Salles G (2016) A Phase 1 clinical trial of the selective BTK inhibitor ONO/GS-4059 in relapsed and refractory mature B-cell malignancies *Blood* **127**:411–419.

Wang ML, Rule S, Martin P, Goy A, Auer R, Kahl BS, Jurczak W, Advani RH, Romaguera JE, Williams ME, Barrientos JC, Chmielowska E, Radford J, Stilgenbauer S, Dreyling M, Jedrzejczak WW, Johnson P, Spurgeon SE, Li L, Zhang L, Newberry K, Ou Z, Cheng N, Fang B, McGreivy J, Clow F, Buggy JJ, Chang BY, Beaupre DM, Kunkel LA, and Blum KA (2013) Targeting BTK with ibrutinib in relapsed or refractory mantle-cell lymphoma *N Engl J Med* **369**: 507–516.

Wang ML, Blum KA, Martin P, Goy A, Auer R, Kahl BS, Jurczak W, Advani RH, Romaguera JE, Williams ME, Barrientos JC, Chmielowska E, Radford J, Stilgenbauer S, Dreyling M, Jedrzejczak WW, Johnson P, Spurgeon SE, Zhang L, Baher L, Cheng M, Lee D, Beaupre DM, and Rule S (2015) Long-term

follow-up of MCL patients treated with single-agent ibrutinib: updated safety and efficacy results *Blood* **126**: 739–745.

Whang JA and Chang BY (2014) Bruton's tyrosine kinase inhibitors for the treatment of rheumatoid arthritis *Drug Discov Today* **19**: 1200–1204.

Winkelstein JA, Marino MC, Lederman HM, Jones SM, Sullivan K, Burks AW, Conley ME, Cunningham-Rundles C, and Ochs HD (2006), X-linked agammaglobulinemia: report on a United States registry of 201 patients *Medicine* **85**: 193–202.

Zapf CW, Gerstenberger BS, Xing L, Limburg DC, Anderson DR, Caspers N, Han S, Aulabaugh A, Kurumbail R, Shakya S, Li X, Spaulding V, Czerwinski RM, Seth N, and Medley QG (2012) Covalent Inhibitors of Interleukin-2 Inducible T Cell Kinase (Itk) with Nanomolar Potency in a Whole-Blood Assay *J Med Chem* **55**: 10047–10063.

FOOTNOTES

This article reveals the reflections of the authors on some of the research and data regarding acalabrutinib. This research has spanned many years and is ongoing. This article does not attempt to address exhaustively every aspect and detail of that research. Financial Disclosures: All authors are employees or consultants of the company, and are shareholders of Acerta Pharma B.V.

FIGURE LEGENDS

Fig. 1. (Left) Chemical structures of clinical irreversible binding BTK inhibitors. (Top right) Front view of a binding model of acalabrutinib (gold) in the ATP binding pocket of BTK. (Bottom right) Second view of the model, showing the hydrogen bonding interaction of the 2-pyridylamide moiety with Ser538 and Asp539.

Fig. 2. (A) Chemical structures of compounds **4** – **9**. (B) Average t½ determination in a pseudo-first order glutathione (GSH) reactivity assay. In brief, the compounds were incubated with an excess of GSH at 37°C and pH 7.4 in a buffered aqueous methanol mixture. Consumption of the electrophilic parent compound was monitored via reversed phase HPLC, and the t½ (50% of parent consumed) was determined based on linear regression analysis from two independent experiments. (Table) Biochemical IMAP and cell-based data for compounds **1** – **9**, and GSH reactivity data for selected compounds.

Fig. 3. Comparison of acalabrutinib, ibrutinib and spebrutinib in competitive binding assays on wild type and mutant kinases (DiscoveRx). Compounds were tested at a single concentration of 1 µM. Data are expressed as % remaining activity versus control, Size of the circles represents intervals of % remaining activity versus untreated control. Data presented are expansions from Herman et al, in press.

Fig. 4. (A) *In vivo* potency: Mice (5 per group) were given an oral dose of acalabrutinib, ibrutinib, spebrutinib or vehicle over a concentration range (x-axis). After 3 hours, spleens were extracted and splenocytes stimulated with anti-IgM for 18h, followed by CD69 expression analysis by flow cytometry gated on CD19+ B cells. The CD69 median fluorescent intensity values were normalized as a percent of the vehicle control group and the mean average and SEM were plotted for all mice in each dose cohort. (B) Return of function: Mice (5 per group) received a single, oral, 25 mg/kg dose of acalabrutinib, ibrutinib, spebrutinib or vehicle. Spleens were extracted 3, 6, 12, 18 or 24 hours after dosing and single cell suspensions made. Splenocytes were immediately cultured with anti-IgM for 18 hours, followed by CD69 surface expression measurement by flow cytometry as in panel A. Data shows CD69 expression for each mouse normalized as a percentage of the vehicle control group. Data presented are expansions from Herman et al., in press. (C) BTK target occupancy was measured in the mouse splenocyte samples from the experiment described under B. (D) Structure of the target occupancy probe ACP-4016 (**10**).

Fig. 5. PK vs PD after acalabrutinib dose in healthy human volunteers. (A) Dose-exposure relationship of acalabrutinib in healthy subjects in Study ACE-HV-001. Log/log presentation showing individual AUC0-12 values with median (horizontal line) for a single dose of 2.5, 5, 25, 50, 75 and 100 mg. (B and C) The PD measures, BTK target occupancy and inhibition of anti-IgM-induced CD69 expression were derived from blood samples drawn from each subject 3 and 12 hours after acalabrutinib administration. Each point represents data from an individual blood sample, and each group median represented by a horizontal line. (D) The mean acalabrutinib concentration in plasma (N=6; left axis, light grey) is plotted with median BTK occupancy (N=4; right axis, grey dotted) and median inhibition of BCR-induced CD69 protein expression on B cells (N=5; right axis, black) from individuals who received a single 100 mg dose. The error bars show the SD for acalabrutinib plasma concentration. For the BTK occupancy and CD69 inhibition data, the error bars show the interquartile range. BTK occupancy data is corrected for changes in B cell numbers.

JPET Fast Forward. Published on September 7, 2017 as DOI: 10.1124/jpet.117.242909
This article has not been copyedited and formatted. The final version may differ from this version.

TABLES

Table 1: Mono-therapy clinical stage covalent BTK kinase inhibitors.

Compound	Company	Stage of Development[a]	Primary Therapeutic Area	Ref.
Ibrutinib (Imbruvica)	J&J, Abbvie	Approved	Oncology	Byrd et al., 2015
Acalabrutinib (ACP-196)	Acerta Pharma	Ph 3	Oncology	Byrd et al., 2016
BGB-3111	BeiGene	Ph 3	Oncology	Tam et al., 2015
Spebrutinib (CC-292)	Celgene	Ph 2	Autoimmune	Evans et al., 2013
Evobrutinib (M2951)	MerckSerono	Ph 2	Autoimmune	Grenningloh, 2016
PRN-1008	Principia	Ph 2	Autoimmune	Smith et al., 2015
LY3337641 (HM-71224)	Lilly	Ph 2	Autoimmune	Park et al., 2016
M7583	MerckSerono	Ph 1/2	Oncology	Bender et al., 2016
Tirabrutinib (GS-4059)	Gilead	Ph 1	Oncology	Walter et al., 2016
AC-0058TA	ACEA Biosciences	Ph 1	Autoimmune	--

a) Clinicaltrials.gov. Development stage of most advanced clinical programme. Additional potential covalent BTK inhibitors: CT-1530, BMS-986195, and DTRMWXHS-12.

JPET Fast Forward. Published on September 7, 2017 as DOI: 10.1124/jpet.117.242909
This article has not been copyedited and formatted. The final version may differ from this version.

Table 2. IC_{50} determination on cysteine kinases with a cysteine in the same position as Cys481 in BTK.

		1	**2**	**3**	**7**
Kinase	**i+3 residue**	**IC_{50} (nM)**			
BTK	Asn	5.1 ± 1.0	1.5 ± 0.2	2.3 ± 0.5	1.6 ± 0.2
TEC	Asn	126 ± 11	10 ± 2	16 ± 4	41 ± 3
ITK	Asp	>1,000	4.9 ± 1.2	24 ± 2	52 ± 5
BMX	Asn	46 ± 12	0.8 ± 0.1	1.6 ± 0.4	3.3 ± 0.4
TXK	Asn	368 ± 141	2.0 ± 0.3	9.1 ± 2.7	7.6 ± 2.4
EGFR	Asp	>1,000	5.3 ± 1.3	199 ± 35	20 ± 5
ERBB2	Asp	~1,000	6.4 ± 1.8	>1,000	13 ± 3
ERBB4	Glu	16 ± 5	3.4 ± 1.4	49 ± 12	5.3 ± 0.5
BLK	Asp	>1,000	0.1 ± 0.0	131 ± 27	19 ± 4
JAK3	Asp	>1,000	32 ± 15	5.4 ± 1.1	>1,000

BTK and ITK kinase activity was measured using the IMAP assay. For BMX, TXK, EGFR, ERBB2, ERBB4, BLK and JAK3 kinase activity was measured at Thermo Fisher using the Z'-LYTE assay. TEC kinase activity is determined in a Lanthascreen assay. Results are average ± SD of at least three independent experiments.

JPET Fast Forward. Published on September 7, 2017 as DOI: 10.1124/jpet.117.242909
This article has not been copyedited and formatted. The final version may differ from this version.

Table 3. Effect of selected compounds on A431 and Jurkat cell lines, and on human PBMC.

Cmpd	EGF-induced EGFR phosphorylation A431 EC_{50} (nM)[a]	anti-CD3/CD28-induced IL-2 production Jurkat EC_{50} (nM)[b]	anti-CD3-induced CD25 expression PBMC EC_{50} (nM)[b]
1	>10,000	>10,000	>10,000
2	71 ± 14	99 ± 17	257 ± 71
3	4,680 ± 720	150 ± 22	575 ± 60
7	327 ± 2	911 ± 61	2,660 ± 956

a) Results are average ± error of two independent experiments. b) Average ± SD of three independent experiments.

JPET Fast Forward. Published on September 7, 2017 as DOI: 10.1124/jpet.117.242909
This article has not been copyedited and formatted. The final version may differ from this version.

FIGURES

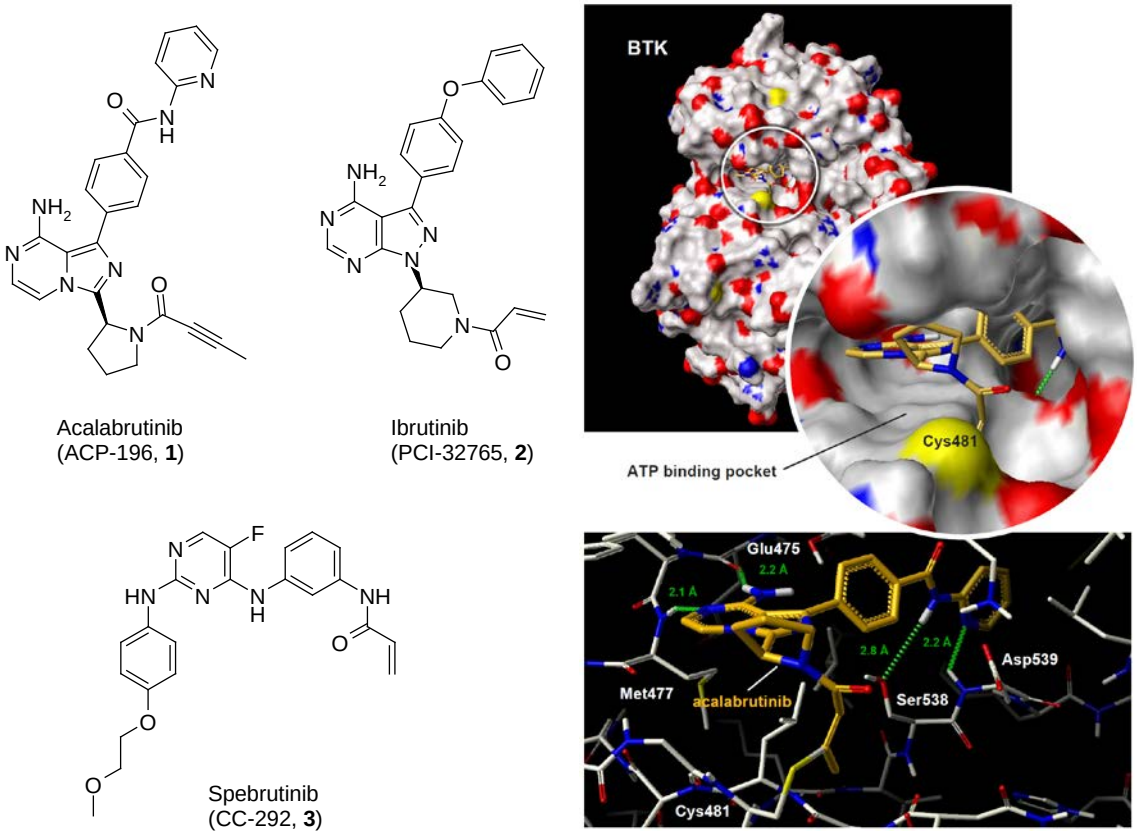

Figure 1

JPET Fast Forward. Published on September 7, 2017 as DOI: 10.1124/jpet.117.242909
This article has not been copyedited and formatted. The final version may differ from this version.

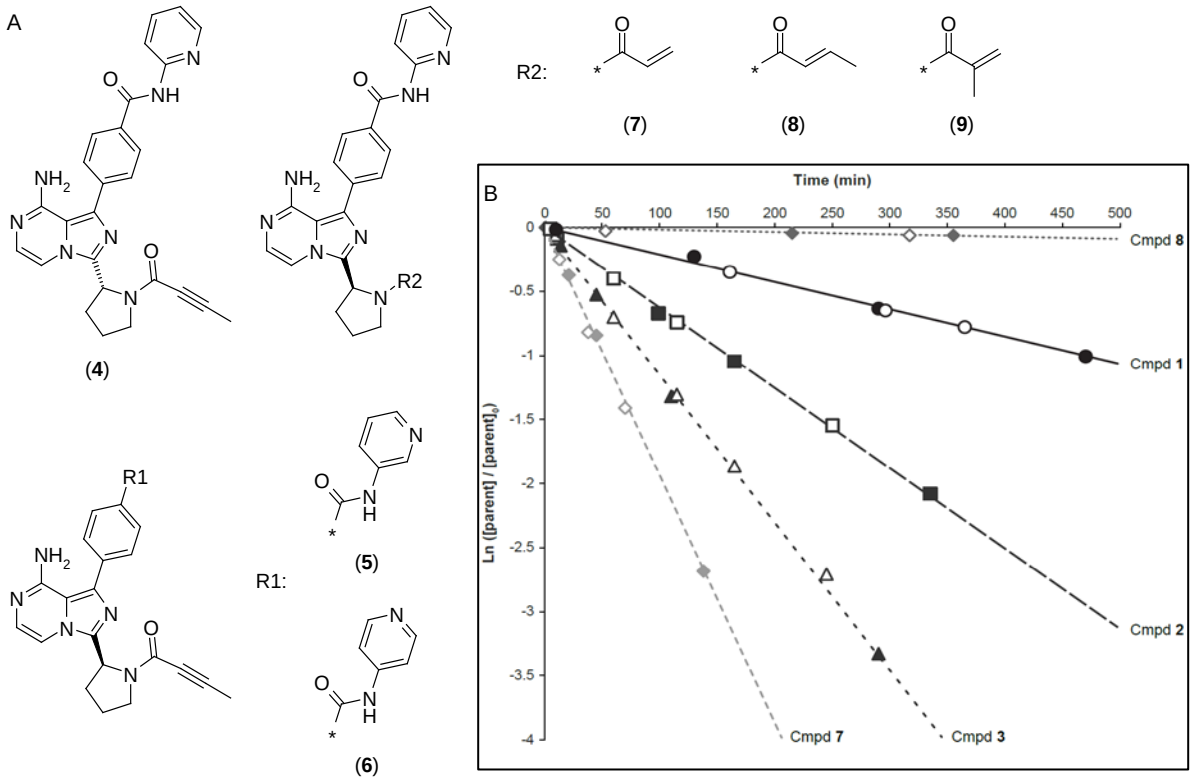

Cmpd	BTK (IMAP) IC_{50} (nM)[a)]	PBMC (CD69) EC_{50} (nM) [a)]	hWB (CD69) EC_{50} (nM) [a)]	GSH reactivity[b)] Average t½ (hour)
1	5.1 ± 1.0	2.9 ± 0.2	9.2 ± 4.4	5.5
2	1.5 ± 0.2	0.58 ± 0.04	5.8 ± 3.0	1.9
3	2.3 ± 0.5	7.4 ± 0.7	140 ± 85	1.0
4	697 ± 157	592 ± 24	1,530 ± 408	--
5	3,970 ± 1,215	>10,000	~10,000	--
6	1,857 ± 300	>10,000	4,210 ± 830	--
7	1.6 ± 0.2	0.82 ± 0.34	2.2 ± 0.3	0.6
8	280 ± 138	119 ± 15	215 ± 62	~95
9	2,517 ± 1,279	1,717 ± 603	1,860 ± 306	No reaction

a) Results are average ± SD of at least three independent experiments. b) Results are average of two independent experiments.

Figure 2

JPET Fast Forward. Published on September 7, 2017 as DOI: 10.1124/jpet.117.242909
This article has not been copyedited and formatted. The final version may differ from this version.

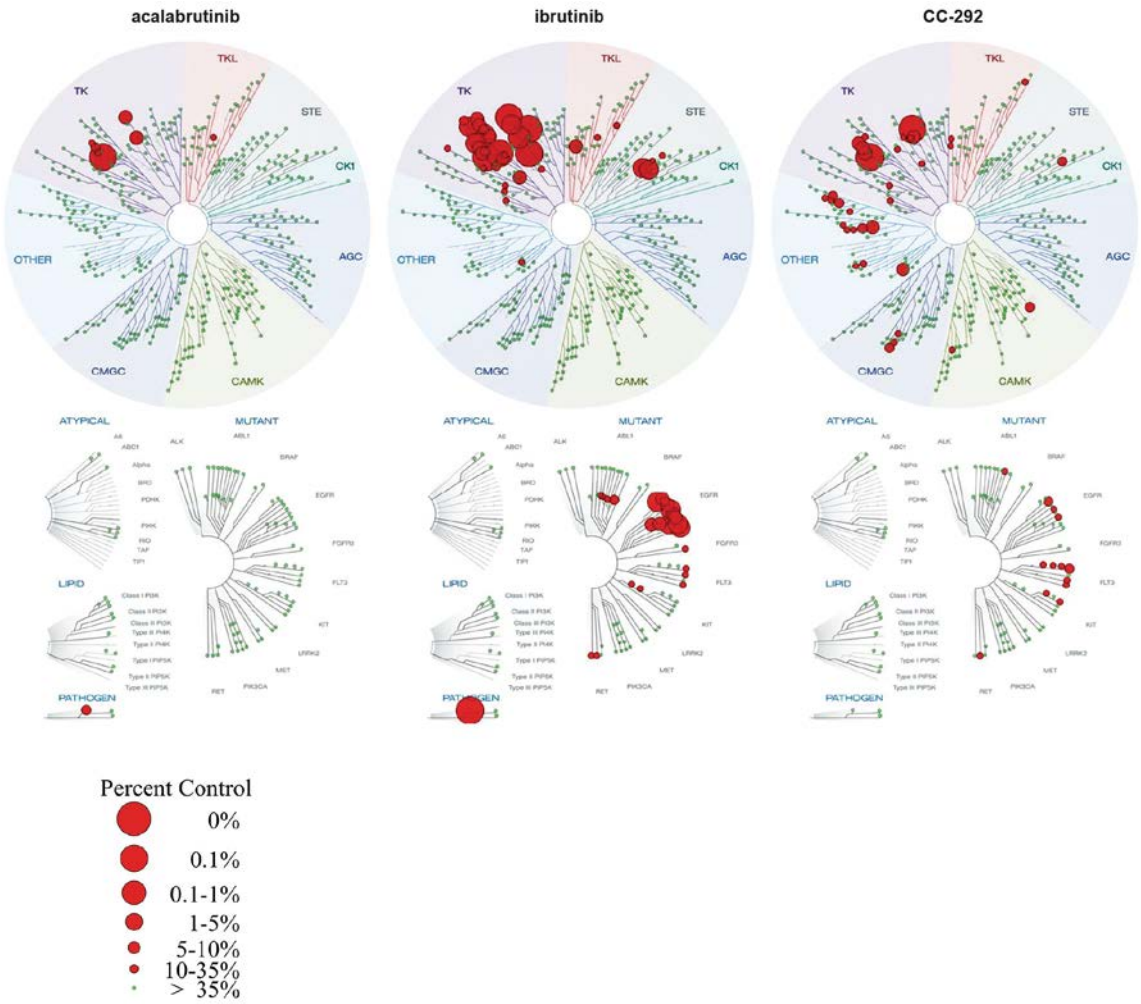

Figure 3

JPET Fast Forward. Published on September 7, 2017 as DOI: 10.1124/jpet.117.242909
This article has not been copyedited and formatted. The final version may differ from this version.

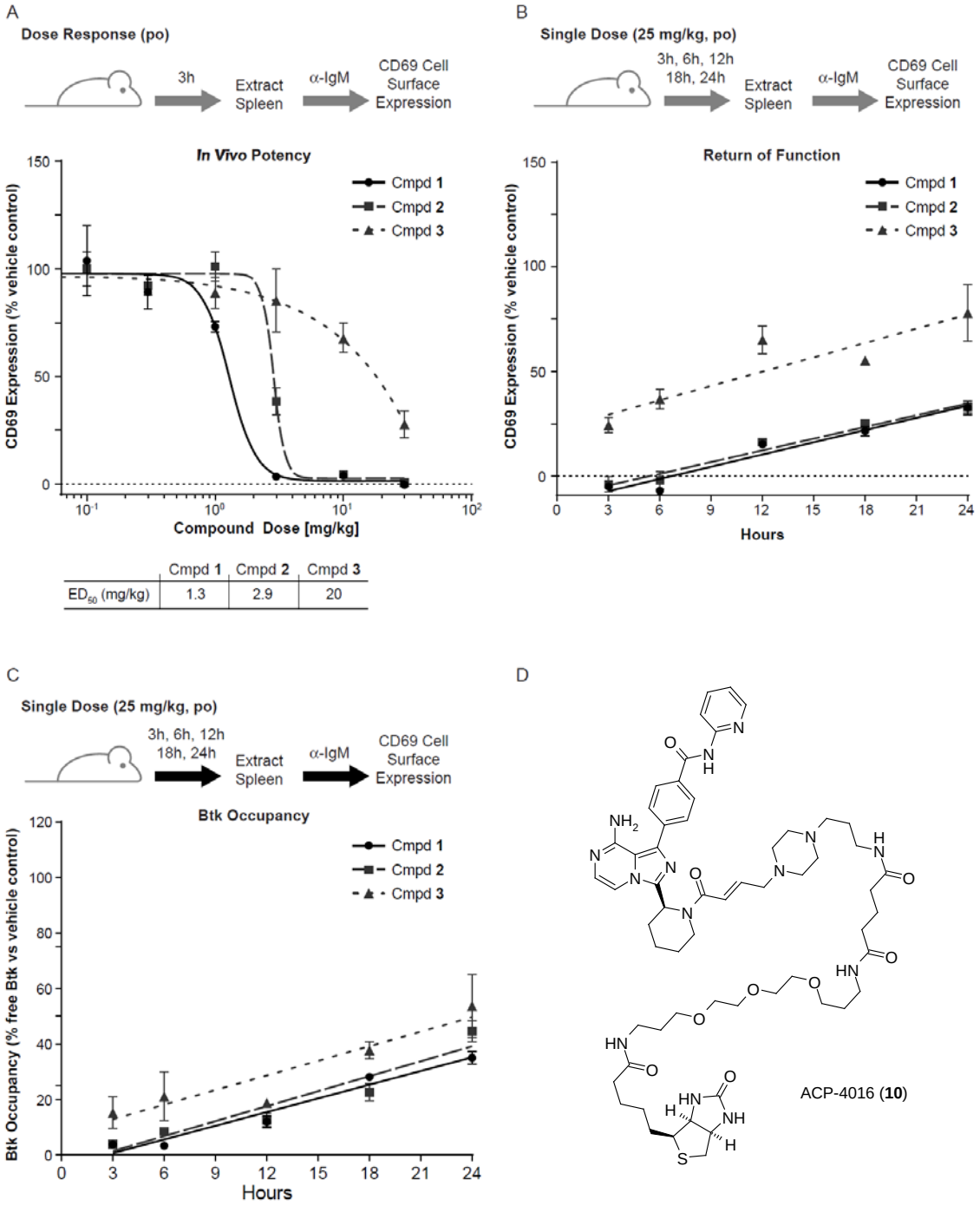

Figure 4

JPET Fast Forward. Published on September 7, 2017 as DOI: 10.1124/jpet.117.242909
This article has not been copyedited and formatted. The final version may differ from this version.

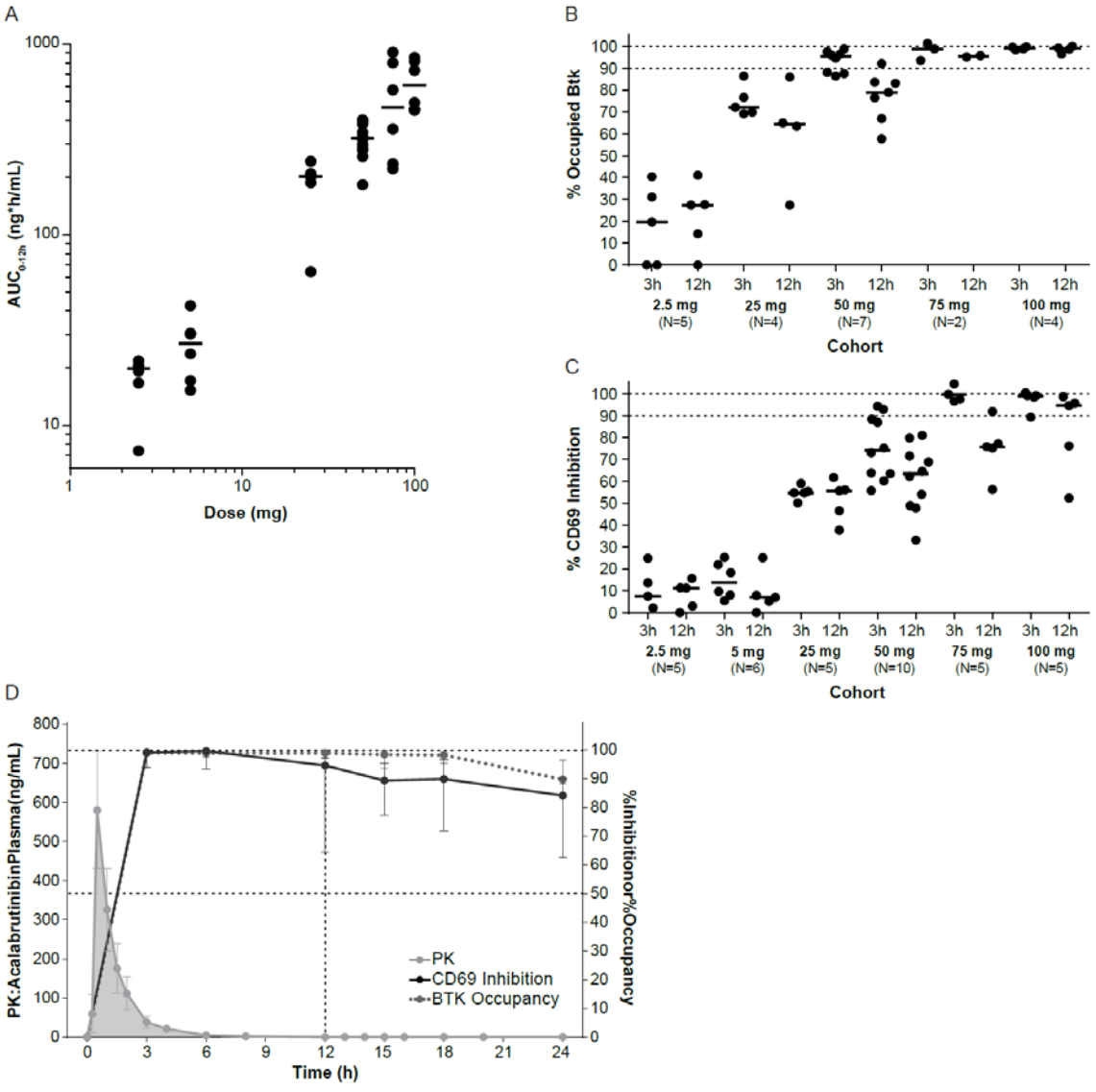

Figure 5